Journal for Geometry and Graphics
Volume 26 (2022), No. 1, 81–100

Geodesic Folding of Regular Tetrahedron

Seri Nishimoto[1], Takashi Horiyama[2], Tomohiro Tachi[1]

[1]*The University of Tokyo, Tokyo, Japan*
s-nishimoto@g.ecc.u-tokyo.ac.jp, tachi@idea.c.u-tokyo.ac.jp

[2]*Hokkaido University, Hokkaido, Japan*
horiyama@ist.hokudai.ac.jp

Abstract. In this paper, we show geometric properties of a family of polyhedra obtained by folding a regular tetrahedron along triangular grids. Each polyhedron is identified by a pair of nonnegative integers. The polyhedron can be cut along a geodesic strip of triangles to be decomposed and unfolded into one or multiple bands. We show that the number of bands is the greatest common divisor of the two integers. By a proper choice of pairs of numbers, a common triangular band that folds into different multiple polyhedra can be created. We construct the configuration of the polyhedron algebraically and numerically through angular and truss models respectively. We discuss the volumes of the obtained folded states and provide relevant open problems regarding the existence of popped-up state. We also show some geometric connections to other art forms.

Key Words: rigid origami, tetrahedron, geodesic bands, basketry

MSC 2020: 51M20

1 Introduction

In this paper, we consider a family of polyhedra obtained by folding a regular tetrahedron along a regular triangular grid. Specifically,we consider a regular triangular grid overlaid on each triangular face of the tetrahedon such that the vertices of the face lie exactly on the grid points. Then,we subdivide the polyhedron along the grid; the subdivision can be identified by two nonnegative numbers a and b. This is a common operation and notation for creating geodesic polyhedra [21]. Folding along the grid while keeping all the faces regular triangles yields a family of (generally) non-convex deltahedra (Figure 1). This is in contrast to the convex geodesic polyhedra, where the vertices are projected on a sphere and thus the triangles are not regular.

Such deltahedral shapes obtained by the subdivision of a regular deltahedron (regular tetrahedron, octahedron, and icosahedron) have been studied in various contexts. Caspar and Klug [8] used them to model viruses, and Kawamura [13] created a modular origami

ISSN 1433-8157/$ 2.50

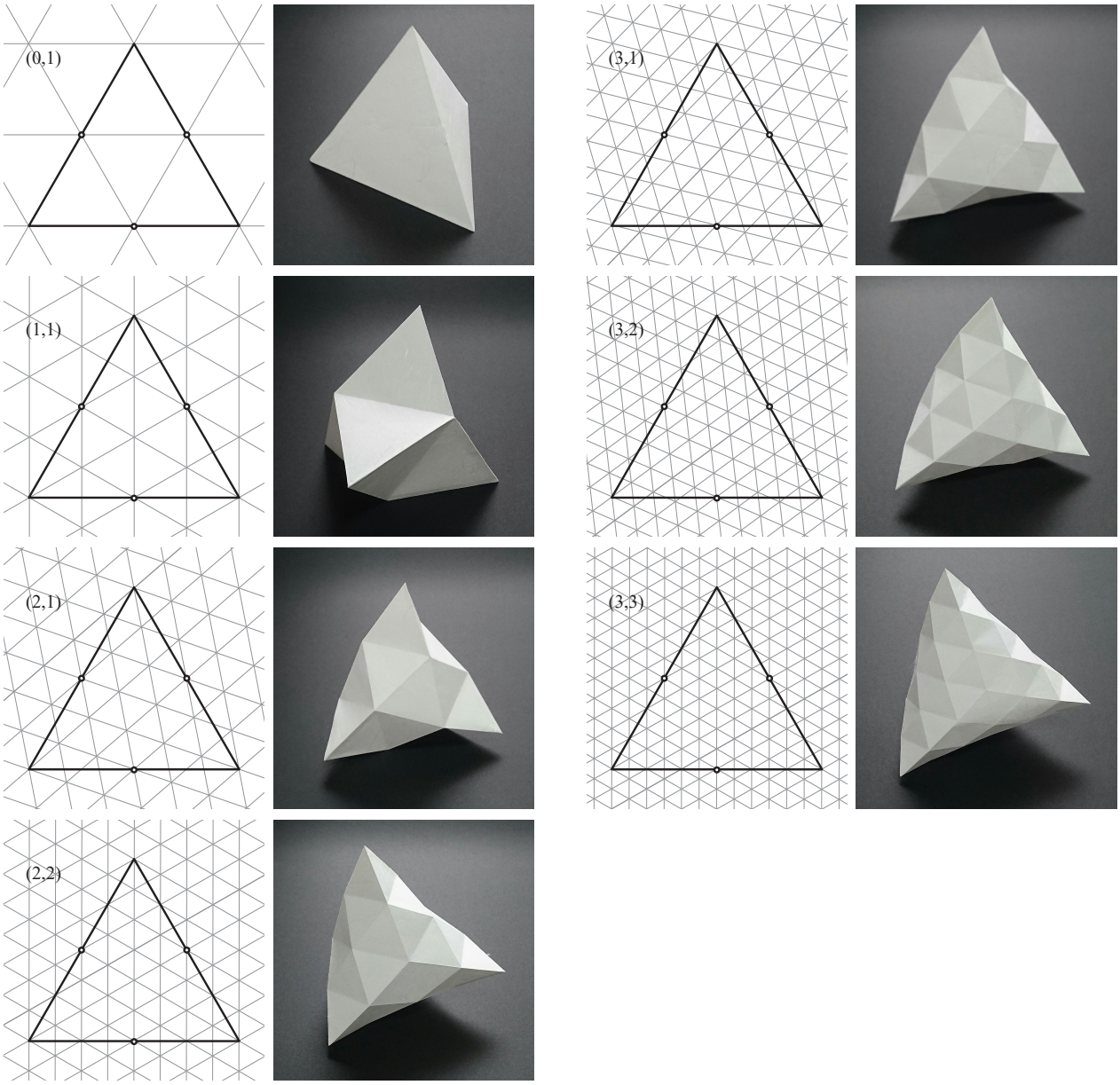

Figure 1: Geodesic foldings of regular tetrahedra. For each pair of (a, b), the left figure shows the development (thick line) with the crease pattern (thin grid) which folds to the model on the right.

artwork called "Geosphere" based on icosahedral models. Gailiunas [11] computed the family of deltahedra obtained by the operation and referred to them as "twisted domes." However, the geometric properties of this family of polyhedra are not yet fully shown. Even its existence, i.e., embedding to Euclidean 3-space, is unknown for a larger a and b (and remains so in this study). We refer to this construction as "geodesic folding"because the subdivision along geodesic lines give shapes isometric to the original polyhedron. In this paper, we focus on the geodesic folding of a regular tetrahedron and show some basic properties of the family.The remainder of this work is summarized as follows.

- Section 2 formalizes the geometry of the geodesic folding.
- Section 3 shows that the geodesic folding of a regular tetrahedron is decomposable into one or multiple triangular bands along the geodesics of the surface and that the number

of bands is the greatest common divisor of a and b.

- Section 3.2 shows multiple types of geodesic folding of tetrahedra that can be folded from the same band.
- Section 4 and section 5 construct the polyhedra embedded in Euclidean 3-space algebraically through an angular model and numerically through a truss model. We discuss the volume-increasing nature of the folding, leading to some open questions regarding the folded states.
- Section 6 discusses the geometric connections between the geodesic folding of tetrahedra and other art forms, namely, triaxial weaving and zippers.

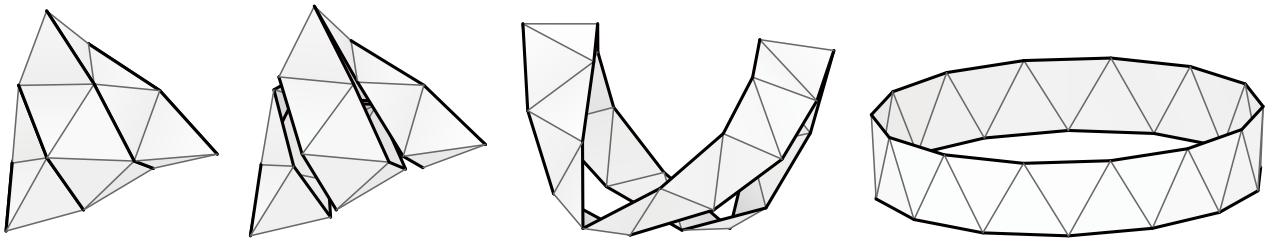

Figure 2: Decomposition of the geodesic folding $(2, 1)$ into a single band of 28 triangles.

2 Basic Geometry

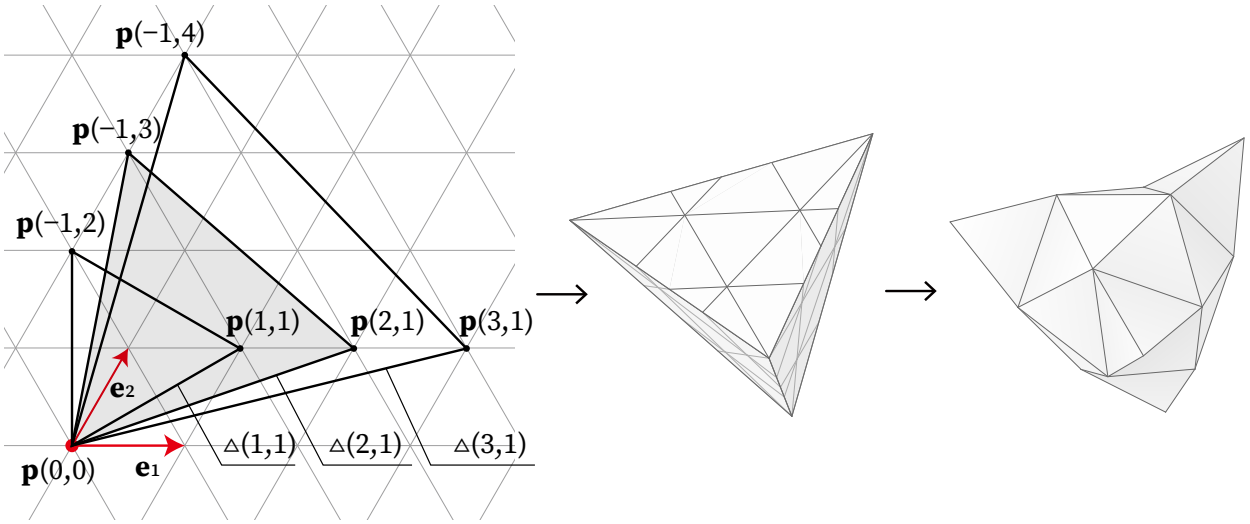

Figure 3: Left: $\triangle(a, b)$ $((a, b) = (1, 1), (2, 1), (3, 1))$ on the equilateral triangular grid, Middle: geodesic crease pattern $(2, 1)$ on the regular triangle. Right: $GFT(2, 1)$.

In this section, we formalize the definition and the procedure. Refer to Figure 3. First, we use the well-accepted notation of *folding* or *folded state*.

Definition 1. A *folded state* is an intrinsically isometric mapping $f\colon P \to \mathbb{E}^3$, where P, referred as a piece of *paper*, is a metric orientable 2-manifold, and $\mathbb{E}^3$ denotes the Euclidean 3D space. Here, intrinsically isometric mapping is a mapping that retains the arclength of any curve on P after the mapping.

Definition 2. A *crease pattern* C on P is a graph embedded on P that partitions P into disjoint open regions, called *faces* of C. A *rigid folded state* of P *using* a crease pattern C is a folded state of P such that for each face P_i, its image $f(P_i)$ is planar.

This implies that when we consider two rigid fold states using a common crease pattern on the same piece of paper, each face between two states can be mapped to one other as a rigid body transformation.

Next, we construct the crease pattern for our problem.

Definition 3. Consider unit vectors $\mathbf{e}_1 = (1, 0)$ and $\mathbf{e}_2 = (\frac{1}{2}, \frac{\sqrt{3}}{2})$ forming 60° on xy-plane. *Grid points* are the set of points $\mathbf{p}(u, v) \coloneqq u\mathbf{e}_1 + v\mathbf{e}_2$ for $u, v \in \mathbb{Z}$. Let an *equilateral triangular grid* be a plane graph whose vertices lie on the grid points and the edges connect all pairs of grid points with distance 1.

Definition 4. An equilateral triangle $\triangle(a, b)$ for nonnegative integers a, b satisfying $(a, b) \neq (0, 0)$ is a triangle region (including the boundary) the vertices of which are on $\mathbf{p}(0, 0)$, $\mathbf{p}(a, b)$, and $\mathbf{p}(-b, a+b)$. The intersection of $\triangle(a, b)$ and the equilateral triangular grid gives a graph embedded on $\triangle(a, b)$, which we call the *geodesic crease pattern* on $\triangle(a, b)$. The geodesic crease pattern (a, b) $(a, b = 0, 1, 2, \dots)$ *on a regular tetrahedron* is the embedding of a graph on the regular tetrahedra given by mapping $\triangle(a, b)$ and its embedded geodesic crease pattern to each face of the tetrahedron by uniform scaling while maintaining the face orientations.

Definition 5. Finally, the *geodesic folding* (a, b) of a regular tetrahedra, denoted by $GFT(a, b)$, is the rigid folded state using the geodesic crease pattern (a, b) on the tetrahedron, i.e., a continuous mapping of the tetrahedron to a 3D Euclidean space in which each face of the graph is isometric to the unit triangle in the image.

Obtaining actual folded states $GFT(a, b)$ in Euclidean 3D space is not trivial. For example, the highlighted triangles in Figure 4 are not in the original position of the tetrahedra; the patches of triangles are not even co-planar. The extrinsic properties of the geodesic folding are covered in Sections 4 and 5, including the computation of the valid folded states. First, we cover the intrinsic properties (considering only the metric along the surface and their connectivity) of $GFT(a, b)$. Here, we present are the basic properties of the geodesic folding of regular tetrahedra (see Figure 4).

Remark 1. $GFT(a, b)$ (intrinsically) has the chiral tetrahedral symmetry. In particular, $GFT(a, b)$ has the full tetrahedral symmetry when $a = b$, $a = 0$, or $b = 0$. (a, b) and (b, a) are mirror-symmetric to each other when $a \neq b$.

By the chiral tetrahedral symmetry, $GFT(a, b)$ can be decomposed into 4 *face patches* and 6 *edge patches*. Here, a face patch is the folding of a $|a - b|$ equal subdivision of a regular triangle, corresponding to the triangle $\mathbf{p}(0, b)\mathbf{p}(a - b, b)\mathbf{p}(0, a)$ into $(a - b)^2$ triangles. An edge patch is a folding of a $a \times b$ parallelogram, corresponding to the parallelogram $\mathbf{p}(0, 0)\mathbf{p}(a, 0)\mathbf{p}(a, b)\mathbf{p}(0, b)$ with $2ab$ triangles.

Remark 2. Each face patch is (intrinsically) 3-fold rotationally symmetric about the corresponding original face center, and each edge patch is (intrinsically) 2-fold symmetric about the midpoint of the corresponding original edge.

Remark 3. The number of triangles on $GFT(a, b)$ is $4(a^2 + ab + b^2)$.

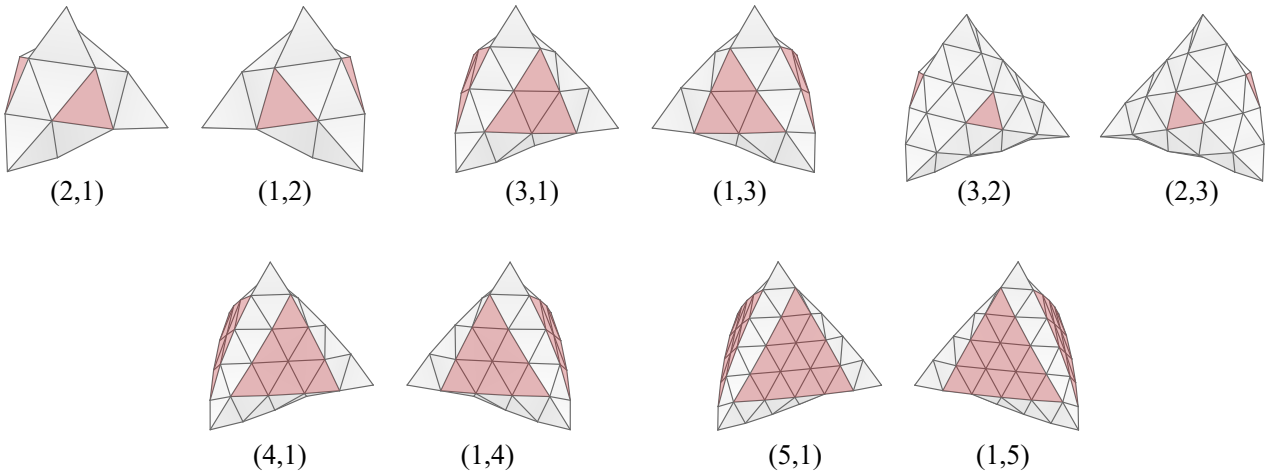

Figure 4: The face patches (highlighted) and the edge patches. Note the chiral symmetry of the geodesic folding.

3 Geodesic Bands

3.1 Decomposition

We now consider the properties of geodesic strip along the geodesic folding of tetrahedra.

Definition 6. A *triangular geodesic strip* on the surface of a tetrahedron is a folding of a $x \times 1$ parallelogram similar to a parallelogram $\mathbf{p}(0,0)\mathbf{p}(x,0)\mathbf{p}(x,1)\mathbf{p}(0,1)$ with $2x$ triangles. We say x to be the *length of* the geodesic strip. *Triangular geodesic band* is a folding of a cylinder composed by connecting the geodesic strip by connecting edges $\mathbf{p}(0,0)\mathbf{p}(0,1)$ and $\mathbf{p}(x,0)\mathbf{p}(x,1)$ in this orientation.

Theorem 1. *$GFT(a,b)$ comprises k disjoint triangular geodesics bands, where k is the greatest common divisor of a and b.*

Proof. This property comes from the tiling property of the unfolding of a regular tetrahedron [2, 3]. Consider a regular triangular grid as in Figure 5, and place the development of the tetrahedron as parallelogram $\mathbf{p}(0,0)\mathbf{p}(2a,2b)\mathbf{p}(2a-b,a+3b)\mathbf{p}(-b,a+b)$, which becomes the motif of the tiling. We construct the tiling of the parallelogram using the $p2$ wallpaper group: specifically, create a copy of the parallelogram rotated by 180° around the midpoint of one of its edges to obtain the union of two developments, and then translate the union by $m\mathbf{u} + n\mathbf{v}(m,n \in Z)$, where $\mathbf{u} = (2a,2b)$ and $\mathbf{v} = (-2b,2a+2b)$ form the bases of the $p1$ wallpaper group. The mapping from a plane to a tetrahedron induced by this tiling is intrinsically isometric; in particular, it preserves the continuity and the tangent continuity (except at the vertices) between the motif.

Because of the intrinsic isometry, a geodesic strip of triangles on the tetrahedral surface can be drawn as a horizontal straight strip, i.e., a parallelogram $\mathbf{p}(0,0)\mathbf{p}(x,0)\mathbf{p}(x,1)\mathbf{p}(0,1)$. We would like to know how (the orientation of the copy of the triangle) and when (the lengths x of the strip) the same triangle appears again.

To find the orientation of the triangles, we first observe that the copies of the same triangle are either translational or 180° rotational copies owing to the $p2$ symmetry (Figure 6). Assume that a single geodesic strip contains 180° rotations of the same triangle. Then, the midpoint of two copies, i.e., the center of rotation, is located at $(a+m\mathbf{u}/2, b+n\mathbf{v}/2)$ $(m,n \in Z)$, which

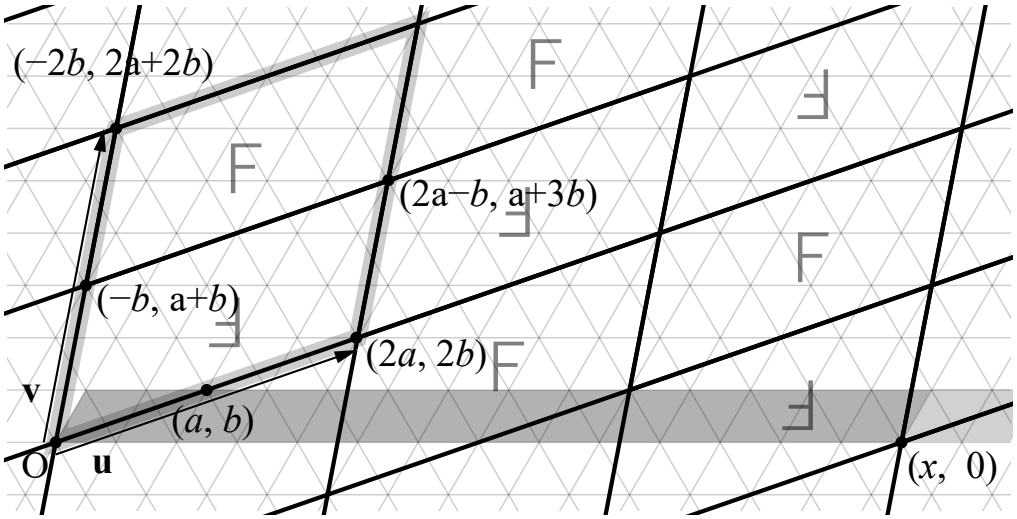

Figure 5: Triangular strip on the tiling of tetrahedra.

is a grid point. Because the geodesic strip does not contain a grid point in the middle, the assumption is contradicted. Hence, the strip hits its translational copy of the first triangle, resulting in the formation of a geodesic band of triangles.

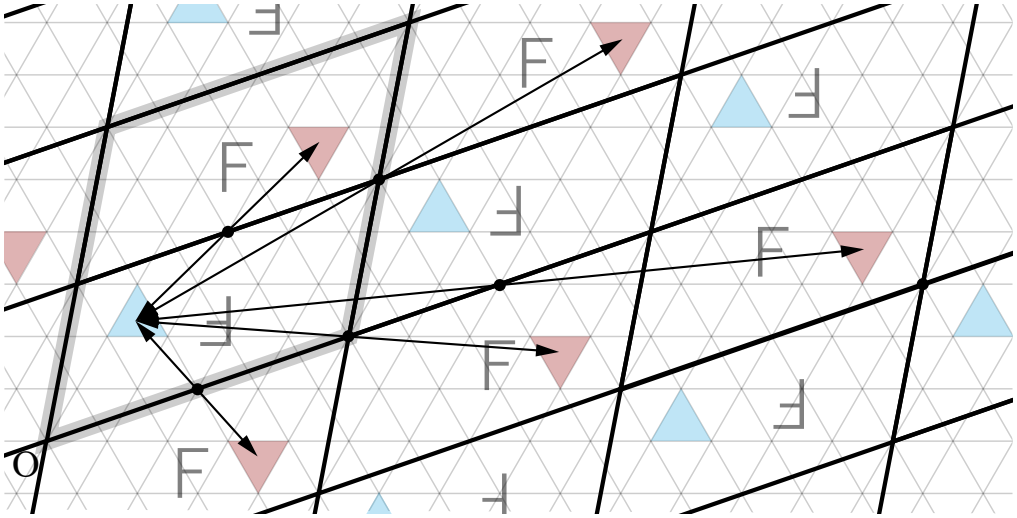

Figure 6: Rotational and translational copies of a triangle.

Here, we find the length x of the strip with $2x$ triangles. The translation from a triangle to its translational copy on the strip can be given by a horizontal vector $(x, 0) = m\mathbf{u} + n\mathbf{v}$. This yields

$$x = 2(am - bn) = 2k(im - jn), \tag{1}$$
$$0 = 2(bm + (a + b)n) = 2k(jm + (i + j)n), \tag{2}$$

where k is the greatest common divisor of a and b, and $i = a/k$ and $j = b/k$. Because i and j are coprime, Equation (2) yields $(m, n) = c(i + j, -j)$ for some integer c. Substituting for m and n in Equation (2) yields $x = 2ck(i^2 + ij + j^2) = \frac{2c}{k}(a^2 + ab + b^2)$. The smallest positive x is given by $c = 1$. The number of triangles in a single band is given by $2x = \frac{1}{k}S(a, b)$ where $S(a, b) = 4(a^2 + ab + b^2)$ is the number of triangles on the tetrahedron. Therefore, the

geodesic folding is decomposed into k bands of equal number of triangles. In particular, if a and b are coprime, the geodesic folding consists of a single band. □

3.2 Common Unfolding

The decomposition into a single band further leads to a new question: can we construct different geodesic foldings of tetrahedra from a common band beyond trivial pairs of (a, b) and (b, a)? The question can be rephrased as that of finding pairs of coprime integers, (a, b) and (a', b') satisfying $S(a, b) = S(a', b')$. We found instances of such numbers by enumerating up to 4×1000000-hedra. We found 45321 instances of geodesic bands that fold into exactly 2 geodesic foldings as given below.

$$\begin{aligned}
\{(1,9),(5,6)\} &\to 4 \times 91,\\
\{(1,11),(4,9)\} &\to 4 \times 133,\\
\{(3,13),(8,9)\} &\to 4 \times 217,\\
\{(3,14),(7,11)\} &\to 4 \times 247,\\
&\dots\\
\{(212,877),(283,828)\} &\to 4 \times 999997.
\end{aligned}$$

We found 9227 instances of geodesic bands that fold into exactly 4 geodesic foldings.

$$\begin{aligned}
\{(3,40),(8,37),(15,32),(23,25)\} &\to 4 \times 1729,\\
\{(4,51),(15,44),(19,41),(25,36)\} &\to 4 \times 2821,\\
\{(2,57),(9,53),(23,43),(33,34)\} &\to 4 \times 3367,\\
&\dots\\
\{(189,892),(276,833),(333,791),(417,724)\} &\to 4 \times 999973.
\end{aligned}$$

We found 318 instances of geodesic bands that fold into exactly 8 geodesic foldings.

$$\begin{aligned}
\{(3,230),(25,218),(43,207),(58,197),(85,177),(90,173),(102,163),(122,145)\} &\to 4 \times 53599,\\
\{(17,244),(31,236),(36,233),(79,204),(83,201),(108,181),(124,167),(141,151)\} &\to 4 \times 63973,\\
&\dots\\
\{(19,990),(55,971),(66,965),(190,891),(446,699),(479,670),(489,661),(555,599)\} &\to 4 \times 999271.
\end{aligned}$$

We did not find any instance that folded into exactly $n \notin \{1, 2, 4, 8\}$ geodesic foldings in this range. The sequence of all numbers with at least two instances is given in the Online Encyclopedia of Integer Sequences as A220171 [19], and the sequence with exactly four instances is given in A198775 [22]. Figure 7 shows the geodesic foldings of tetrahedra $(1, 9)$ and $(5, 6)$ with a common unfolding.

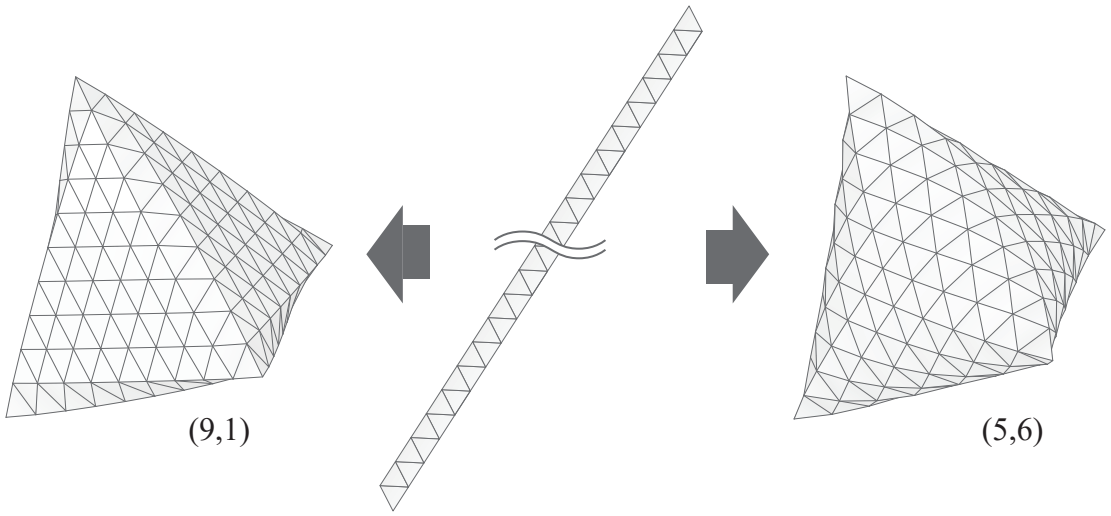

Figure 7: The geodesic foldings of tetrahedron $(1, 9)$ and $(5, 6)$ folded from a common strip.

4 Symbolic Computation of 3D Embedding

The folded state in Euclidean 3-space can be computed using the theory of rigid origami. There are two major approaches: the angular model and the truss model. The angular model represents the folded state by the fold angle of each crease. These angles are constrained for each vertex, forming a cycle of faces connected by creases. The angular model is applied in Sections 4.1 and 4.2 to algebraically compute the possible folded state for $a + b \leq 4$. The truss model, on the other hand, represents the folded state using the coordinates of vertices, which are constrained by preserved edge length. In Section 5, we apply the truss model to numerically compute the folded state for different integers up to $(7, 7)$. (Section 5.2).

Note that the folded form satisfying the isometry is not unique, but has multiple stable positions with versions with dimples (Figure 8). We are interested in the "bulky" or popped-up state, the definition of which is provided in Section 4.2.

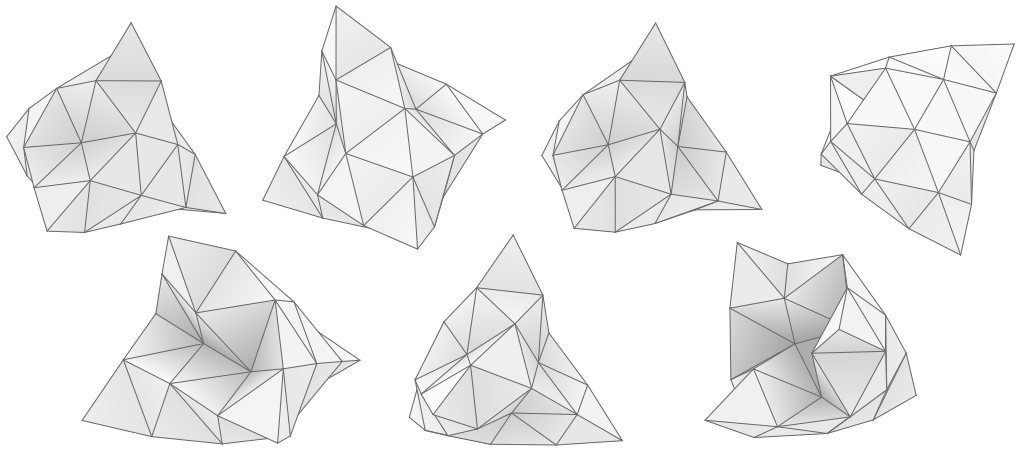

Figure 8: Multiple solutions with "dimples" for $GFT(3, 1)$. We conjecture that the folded shape with all vertices being "popped-up" is unique.

4.1 Basics of Angular Model of Rigid Origami

We first review the rigid origami model using fold angles. Because each face is connected to one another through creases, it is obvious that the fold angles are sufficient to uniquely represent the folded state up to rigid body motion. However, an arbitrary list of fold angles does not necessarily represent a valid folded state, as such construction would produce inconsistency with gaps between faces. The sufficient and necessary condition for a topologically spherical origami to be a valid folded state is stated as follows. For each interior vertex, the product of rotations around the cycle ends in identity [6, 14, 16, 18]. This condition for each vertex is called a *closure constraint*.

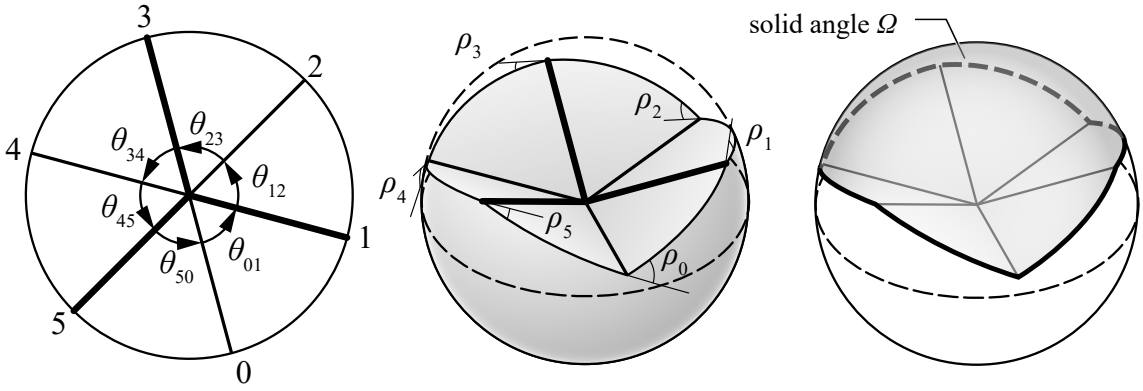

Figure 9: Notation for a single vertex.

Definition 7. Consider a *k-valent*, i.e., a vertex with k incident creases $i = 0, \ldots, k-1$ mod k in counterclockwise order. For each crease, the signed angle between the normal vectors of adjacent faces is called the *fold angle*, where the sign of fold angle is positive or negative if the crease is respectively a valley or mountain viewed from the front side. The fold angle at crease i is denoted by ρ_i. The angle between adjacent creases i and $i+1$ with respect to the vertex, called *sector angle*, is denoted by $\theta_{i,i+1}$.

The product of rotations applied around the cycle of a k-valent vertex can be represented using quaternions as

$$\mathbf{q} \coloneqq \prod_{i=0,\ldots,k-1} \mathbf{q}_x(\rho_i)\mathbf{q}_z(\theta_{i,i+1}), \tag{3}$$

where

$$\mathbf{q}_x(\rho_i) = \cos\frac{\rho_i}{2} + \sin\frac{\rho_i}{2}\mathbf{i}, \tag{4}$$

$$\mathbf{q}_z(\theta_{i,i+1}) = \cos\frac{\theta_{i,i+1}}{2} + \sin\frac{\theta_{i,i+1}}{2}\mathbf{k}, \tag{5}$$

are the quaternions representing the rotations about x and z axes, respectively.

Then, the closure constraint is that the rotation maintains identity, i.e., for any quaternion $\mathbf{p}$ $\mathbf{qpq}^{-1} = \mathbf{p}$, or equivalently,

$$\mathbf{q} = 1, \tag{6}$$

Here, note that because $\mathbf{q}$ is already a unit quaternion by definition (3), it is sufficient to check the three coefficients of the imaginary parts being 0. So, we can rewrite our equation

as

$$\Im\left(\prod_{i=0,\ldots,k-1}(1+t_i^x\mathbf{i})(1+t_{i,i+1}^z\mathbf{k})\right)=\mathbf{0}, \tag{7}$$

where $t_i^x \coloneqq \tan\frac{\rho_i}{2}$ and $t_{i,i+1}^z \coloneqq \tan\frac{\theta_{i,i+1}}{2}$. Note that we multiplied each quaternion by $\cos\rho_i$ or $\cos\theta_{i,i+1}$, to preserve the imaginary part.

Equation (7) forms a system of simultaneous polynomial equations by taking t_i^x as variables with given constants $t_{i,i+1}^z$. The solution of such a system forms an algebraic variety, and thus can be algebraically computed through the computation of the Gröbner basis. We used *Mathematica* to solve the closure constraint.

4.2 Symbolic Computation with Angular Model

Strategy For the geodesic folding of tetrahedra, all sector angles are $\frac{\pi}{3}$, i.e., $t_{i,i+1}^z = \frac{1}{\sqrt{3}}$. We simultaneously solve for t_i^x for every vertex in this system. As the symbolic computation of polynomial equations tends to stop working with less than ten variables and equations, we reduced the number of variables by applying the chiral tetrahedral symmetry in the folded state. Specifically, we assume that the corresponding creases in the symmetry have the same fold angles and thus valuate the constraints only around unique vertices up to the symmetry. Figure 10 shows unique creases and vertices for models of $(1,1)$, $(2,1)$, $(2,2)$, and $(3,1)$ under the symmetry.

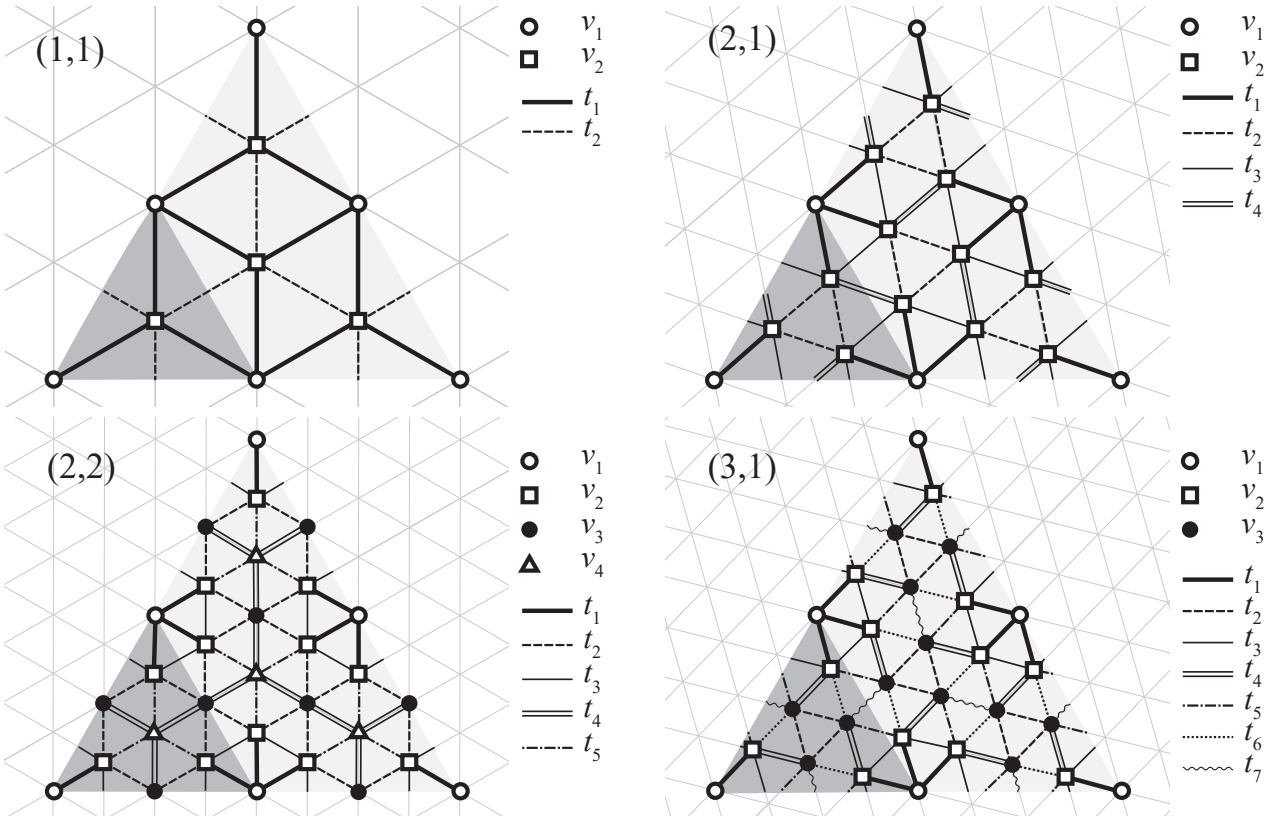

Figure 10: Unique creases and vertices for models $(1,1)$, $(2,1)$, $(2,2)$, and $(3,1)$. Open circle and bold solid line consist of the corners of tetrahedra, so the fold angle is the negative Maraldi angle.

For example, $(1,1)$ has two independent creases with tangent half-fold angles t_1 and t_2, respectively represented as bold solid and dashed lines, and two independent vertices v_1 and v_2, respectively represented by open circles and open squares. Because the corner vertex v_1 is the corner of a regular tetrahedron, the fold angles of incident edges have a negative Maraldi angle, i.e., $t_1 = -\sqrt{2}$. By computing the equation for v_2, we obtain the solutions $t_2 = -\sqrt{2}, \frac{\sqrt{2}}{5}$. Note that the first solution with all creases with $-\sqrt{2}$ tangent half angle is persistent in every system of (a,b) as it represents the trivial solution with self-intersecting multiple coverings of the unit tetrahedron. We obtain the desired folded state with $t_2 = \frac{\sqrt{2}}{5}$ for $(1,1)$, which matches the known state constructed by four regular tetrahedra attached to a regular tetrahedron.

We can similarly obtain 6 solutions for $(2,1)$, 16 solutions for $(2,2)$ and 12 solutions for $(3,1)$ in a symbolic form. These solutions represent different valid states folded from the same pattern with potential self-intersection. Here, in our study, we are interested in an intersection-free *popped-up* folded state among these solutions, which is defined as follows.

Popped-up and Popped-down Solutions

Definition 8. The folded state around a vertex is *popped up* or *popped down* if the fold angles of incident creases sum to $(-2\pi, 0)$ or $(0, 2\pi)$ respectively, i.e.,

$$\sum_{i=0,\ldots,k-1} \rho_i \in (-2\pi, 0) \quad \text{or} \quad (0, 2\pi), \tag{8}$$

respectively. The folded state is *popped-up* or *popped-down* if every vertex is popped up or popped down, respectively.

The geometric interpretation of the criteria is as follows. We can consider the intersection of the folded state with a small sphere centered at a vertex, and scaling the sphere into a unit sphere. If the folded state is free of self-intersection, the sphere is divided into exterior and interior regions; we call the area of the former the *exterior solid angle* of the vertex and denote it by Ω (Figure 9). By the Gauss-Bonnet theorem on a sphere, the total turn angles, i.e., the sum of fold angles, measures the solid angle, so

$$\sum_{i=0,\ldots,k-1} \rho_i = 2\pi - \Omega. \tag{9}$$

Therefore, the vertex is popped-up (or popped-down, resp.) if the vertex has less (or more, resp.) interior than exterior solid angles. Also, a vertex not either popped-up or down ($\sum_{i=0,\ldots,k-1} \rho_i \in (\infty, -2\pi)$ or $(2\pi, \infty)$) is self-intersecting. Furthermore, for an origami vertex that is developable or exhibits positive Gaussian curvature, the folded state exists in an half-space separated by a plane passing through the vertex. In this case, the popped-up and popped-down states corresponds to which of the half-spaces the folded state exists [1].

4.3 Results

We filtered out the folded form that are not popped up. This results in unique solution for each of $(2,1)$, $(2,2)$, and two solutions for $(3,1)$. The symbolic solution for $(2,1)$ is given by

$$\begin{pmatrix} t_1 \\ t_2 \\ t_3 \\ t_4 \end{pmatrix} = \begin{pmatrix} -\sqrt{2} \\ \frac{-3+\sqrt{5}}{2} \\ \frac{\left(\sqrt{2}-1\right)\left(\sqrt{5}-1\right)}{2} \\ \frac{-3+\sqrt{5}}{2} \end{pmatrix}, \tag{10}$$

which coincides with the solution given by the union of a regular icosahedron and four regular tetrahedra. Note the mirror-symmetry around v_2, i.e., $t_2 = t_4$. This is derived locally around v_2; specifically, mirror symmetric partial sequence of t_3, t_1, t_3 induces the mirror symmetry of four triangles about crease corresponding to t_1; this forces the remaining two triangles and thus the sequence t_2, t_2, t_4 to also be mirror-symmetric.

The symbolic solution for $(2, 2)$ was computed as the root of 6-th order equations,the numerical values of which are

$$\begin{pmatrix} t_1 \\ t_2 \\ t_3 \\ t_4 \\ t_5 \end{pmatrix} \approx \begin{pmatrix} -\sqrt{2} \\ -0.2725490570331479 \\ 0.2084858065880353 \\ 0.13627452851657396 \\ -0.5408997896537101 \end{pmatrix}. \tag{11}$$

For the folded state of $(3, 1)$, we first use the above-mentioned mirror symmetry constraints around vertex v_2; from the mirror-symmetric partial sequence t_3, t_1, t_3, we derive $t_4 = t_5$. Then, we solved the closure constraint to obtain two popped up configurations as the solutions to the 30-th order equations, whose numerical values are

$$\begin{pmatrix} t_1 \\ t_2 \\ t_3 \\ t_4 \\ t_5 \\ t_6 \\ t_7 \end{pmatrix} \approx \begin{pmatrix} -\sqrt{2} \\ -0.03889082106629427 \\ 0.20808062128202368 \\ -0.2717704068147588 \\ -0.2717704068147588 \\ -0.5422356969347987 \\ 0.21335302931710964 \end{pmatrix}, \begin{pmatrix} -\sqrt{2} \\ 0.636512482922713 \\ 0.004483554358124968 \\ -2.814848532296878 \\ -2.814848532296878 \\ 1.387606732585032 \\ -0.02524094737550236 \end{pmatrix}. \tag{12}$$

Figure 11 shows the folded states using the list of angles. The second solution of $(3, 1)$ is self-intersecting, and thus the first solution is the desired one.

Theorem 2. *There is a unique popped-up state of $GFT(a, b)$ without intersection for $a + b \leq 4$.*

This leaves the following open problem.

Problem 1. Does a popped-up state of $GFT(a, b)$ without intersection always exist for any integers $a + b > 4$? Is the solution unique?

From the numerical computation shown in the next section, we conjecture the existence of such a state. On the other hand, the uniqueness does not seem to be intuitive and there may be counterexamples for larger a and b.

5 Numerical Computation of 3D Embedding

To create a geodesic folding for larger integers, we created a truss model, or a pin-jointed-framework, in which the vertices are connected by ridges that retain their length. We solved the truss model numerically; a similar approach was used to find deltahedral forms from generated graphs [17]. We generated an initial configuration of the truss with the correct topology from integers a and b and modified the lengths of the edges through an iterative method. Specifically, we constructed a mass-and-spring model and solved its equilibrium based on a dynamic relaxation method. We implemented the parametric construction of the initial configuration using the *Grasshopper* on *Rhinoceros* as the platform and the subsequent dynamic relaxation using the *Kangaroo2* [20] component.

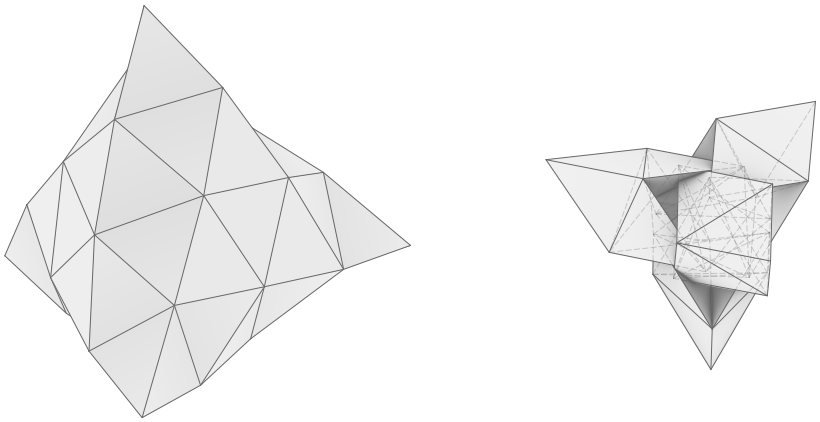

Figure 11: Two popped-up solutions of $GFT(3,1)$. Left and right images correspond to the first and second solutions of Equation (12), respectively. The second solution has a heavy self-intersection.

5.1 Optimization

Initial Configuration First, we computed the initial configuration with correct topology. We constructed triangles on face and edge patches (Figure 12). We constructed a face patch on the triangular face of the original tetrahedron at the original position of the corresponding region in the face.

The construction of the face patch also computes the boundary positions of the edge patch. We constructed the edge patch as the interpolation between face patches. Let the four corner points of an edge patch be $\mathbf{x}_1$, $\mathbf{x}_2$, $\mathbf{x}_3$, and $\mathbf{x}_4$. Then the initial positions of vertices in the edge patch are obtained by bi-linear interpolation satisfying $\mathbf{x}(0,0) = \mathbf{x}_1$, $\mathbf{x}(a,0) = \mathbf{x}_2$, $\mathbf{x}(0,b) = \mathbf{x}_3$, $\mathbf{x}(a,b) = \mathbf{x}_4$, which are given as follows.

$$\mathbf{x}(m,n) = \frac{b-n}{b}\left\{\frac{(a-m)\mathbf{x}_1}{a} + \frac{m\mathbf{x}_2}{a}\right\} + \frac{n}{b}\left\{\frac{(a-m)\mathbf{x}_3}{a} + \frac{m\mathbf{x}_4}{a}\right\}, \tag{13}$$

where $m = 0, 1, 2, \ldots, a$ and $n = 0, 1, 2, \ldots, b$. We constructed a triangular mesh given by combining the face and edge patches.

Objective Function We consider a mass spring system by replacing each edge of the polyhedron as a spring with natural length $\ell = 1/\sqrt{a^2 + ab + b^2}$ and each vertex with a unit mass. Let V and E denote the sets of vertices and edges, respectively. The vertex coordinates are the variables, represented by $\mathbf{X} = \left[\mathbf{x}_1^\mathsf{T}, \ldots, \mathbf{x}_{|V|}^\mathsf{T}\right]^\mathsf{T}$, where $|V|$ is the number of vertices given by $|V| = 2(a^2 + ab + b^2) + 2$.

To obtain the state with popped-up state, we also introduce internal pressure to gently inflate the tetrahedron. The overall problem reduces to a problem of minimizing the total energy U,

$$U = w_{\text{spring}} U_{\text{spring}} + w_{\text{volume}} U_{\text{volume}}, \tag{14}$$

where, U_{spring} and U_{volume} are the potential energy of the springs and internal pressure, respectively. Also, w_{spring} and w_{volume} are the weights of the corresponding energies.

Spring U_{spring} is the sum of the potential energy of the springs. Potential energy for each spring between vertices u and v is defined by $U_{u,v} \coloneqq \frac{1}{2}\left(\|\mathbf{x}_u - \mathbf{x}_v\| - \ell\right)^2$ and U_{spring} is

given by $U_{\text{spring}} = \sum_{(u,v)\in E} U_{u,v}$. We used the *Length(Line)* goal object in Kangaroo2 to model the springs.

Volume U_{volume} is the potential energy by the internal pressure. We assume constant internal pressure of P,and so the potential energy is then given by $U_{\text{volume}} = -PV$. We used the *Pressure* goal object in Kangaroo2 to model the pressure.

Optimization We used the *Solver* component in Kangaroo2, to compute the equilibrium. The weight w_{volume} is initially determined such that every vertex is popped up. However, with the existence of pressure, the result may not be accurately isometric to the original tetrahedron. So, when the shape reached an equilibrium, we gradually decreased w_{volume} to 0.

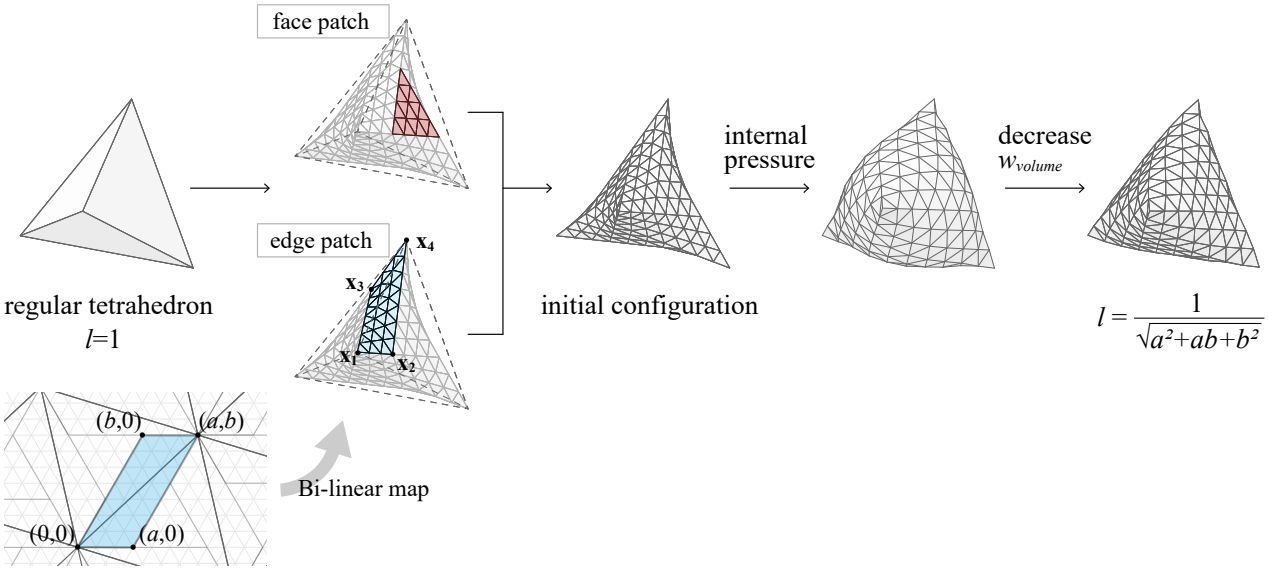

Figure 12: Numerical computation workflow for the truss model.

5.2 Results

The results of the truss-based numerical computation is shown in Figure 13. We confirmed that the error in the edge lengths of the computed model was on the order of 10^{-14} using double precision floating point coordinates for the vertices. Also, the shape obtained by this approach was confirmed to be a popped-up state by computing Equation (9) in the range of Table 1. Note that geodesic foldings with larger a and b have almost flat regions, e.g., $(a, b) = (1, 7)$ has a vertex with $\sum \rho \approx 3 \times 10^{-5}$. Therefore, the judgment of pop-up and pop-down may be affected by the precision for higher numbers than those we computed.

We also computed how the volume of the geodesic foldings of tetrahedra changes by changing the integer pairs a and b. Table 1 shows the relative volumes computed by the numerical method with respect to the regular tetrahedron. We found that, except for $(1, 1)$, the volumes were larger than the original tetrahedron. However, the volume did not continue to increase with increasing numbers. From this study, we identified the volume that takes a local maximum at $(5, 5)$. Note that this was still a numerical computation, and our observation is limited to $a, b \leq 7$. Whether $(5, 5)$ has the globally maximum volume remains as an open question.

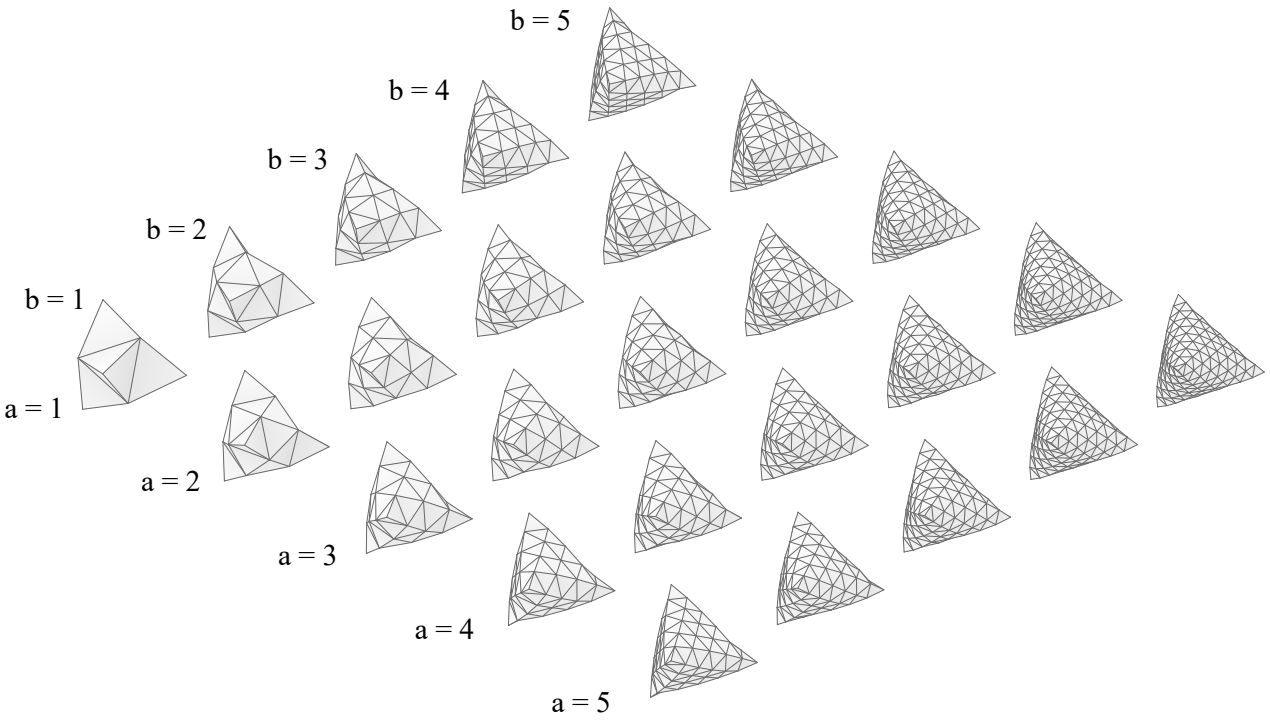

Figure 13: Numerically computed solutions using truss method.

In an attempt of obtaining popped-up states, we accidentally found examples of geodesic foldings that were not popped-up but had larger volumes than their popped-up state. Figure 14 shows such examples. This leads to a question of finding the maximum volume allowing a geodesic folding to be not popped up.

Problem 2. Find the maximum volume state of GFTs.

The problem is a special version of volume increasing isometric deformation [7].

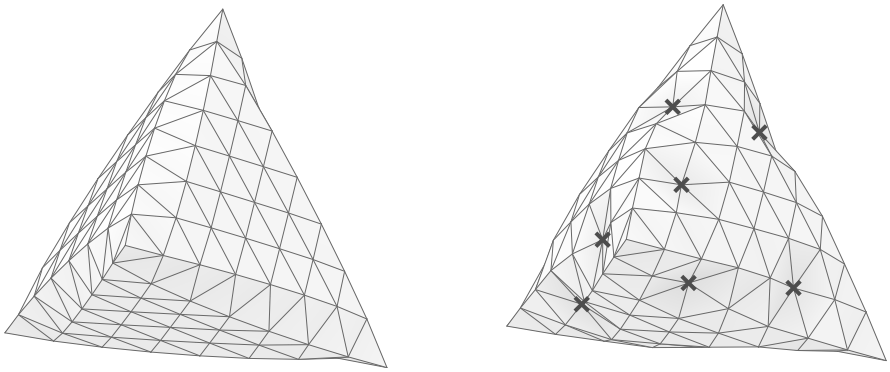

Figure 14: Example of geodesic foldings of tetrahedra that are not popped up but have lager volume than their popped-up states. Left: Popped-up state of $GFT(1,7)$ (volume: 1.27254). Right: $GFT(1,7)$ with popped-down vertices (volume: 1.321687). The cross marks indicate popped-down vertices.

Table 1: Volumes of computed geodesic folding. Every folded state was confirmed to be popped up. $(5, 5)$ takes a local maximum volume.

a\b	1	2	3	4	5	6	7
0	1	1	1	1	1	1	1
1	0.96225	1.21555	1.305946	1.318388	1.309293	1.291614	1.27254
2		1.29799	1.360066	1.386255	1.388193	1.379776	1.364827
3			1.391266	1.409836	1.415833	1.411978	1.402804
4				1.422139	1.426613	1.424967	1.41858
5					**1.43013**	1.429054	1.424419
6						1.428434	1.424969
7							1.4225

6 Geodesic Strip for Fabrication

This section shows the geometric connections between the geodesic band property of our polyhedra and other forms of art and fabrication.

6.1 Triaxial Weaving

Triaxial kagome weaving of straight strips is a traditional technique for basketry. The weaving technique has been also applied to the fabrication of architectural-scale structures as this allows complex curved surfaces to be constructed from straight materials [5]. Whereas a planar weaving pattern consists of a tessellation of hexagonal holes; nondevelopable surfaces can be created by replacing the hexagons with other polygons to create defects at some singular points. If hexagons are replaced by pentagons or quadrangles, the surface obtains positive curvature, leading to traditional basketry; if they are replaced by heptagons and octagons, the surface obtains negative curvature [4]. By removing the edge of the holes by 12 in total[1], we can create closed shapes homeomorphic to a sphere. A tetrahedron can be woven from strips by placing four singular points with triangular holes [12].

This weaving system is related to the geodesic folding of tetrahedra. By replacing each face of the geodesic folding of tetrahedron with a pattern as shown in the Figure 15, we can obtain triaxial weave structures as shown in Figure 16. Because the woven strips align with three possible directions for decomposing the polyhedron into strips, each polyhedron uses only $3k$ bands, where k is the GCD of two integers.

6.2 Zipper

Fabrication using zippers is used as the method to quickly assemble and disassemble three dimensional forms [15]. By attaching the zippers to the development of a shape, we can specify which part of the boundaries are glued together. This is equivalent to specifying the gluing tree for a polygonal development to create different polyhedra [9][10, Chapter 25], although in our cases, the resulting shapes need not be convex.

The geodesic folding of tetrahedra can be applied to create zippered tetrahedra shown in figure 17. Because it develops into a band, the tetrahedral shape is made of a single looped

[1]The total defect angle must be 4π for a topological sphere owing to the Gauss-Bonnet theorem, which is achieved by removing 12 times $\frac{\pi}{3}$.

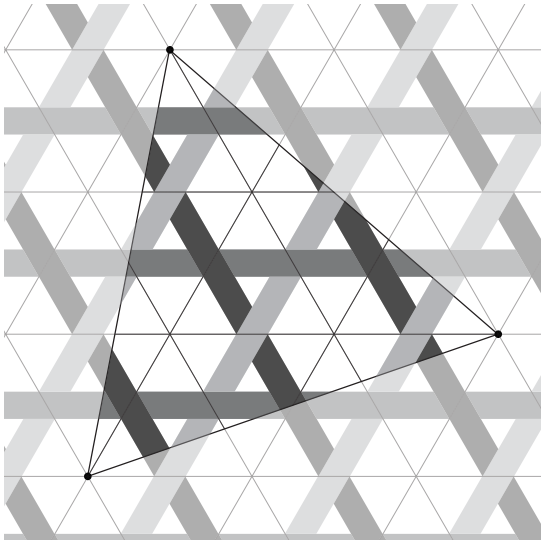

Figure 15: Kagome weave pattern

(a) $(1,1)$ (b) $(1,2)$ (c) $(1,3)$ (d) $(1,4)$

Figure 16: Kagome weaving created from geodesic folding of tetrahedron. The integers indicate the integers of the base geodesic folding of tetrahedron. Note that each model is made of three strips.

strip with zipper fasteners attached on each side as shown in figure 18. The loop on each side is split in half, and they are attached by a zipper from one end to the other as shown in figure 19. This corresponds to a gluing tree as a path between the end points. As these ends form the vertices of the base tetrahedron, their relative positions on both sides are determined by the pair of integers of base geodesic folding. If the unfolding has a different folding as mentioned in 3.2, we can make several different polyhedra from the same loop by changing the end points of the zipper.

7 Conclusion

In this paper, we presented the properties of the geodesic folding of a tetrahedron. First, we showed that the geodesic folding of regular tetrahedra is decomposable into one or multiple triangular bands along the geodesics of the surface, and the number of bands is the greatest common divisor of a and b. Next, we found that multiple instances of geodesic foldings can be folded from the same band. Then, we algebraically constructed the geodesic folding in 3D

(a) $(2,1)$ (b) $(3,1)$ (c) $(4,1)$

Figure 17: Zippered tetrahedra created from geodesic folding of tetrahedron. The integers indicate the integers of base geodesic foldings. Each model was made from a single looped strip.

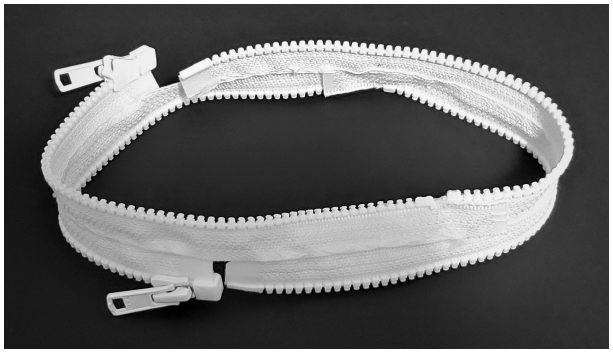

Figure 18: Looped strip with zipper fasteners attached on each side. This loop creates a tetrahedron based on GFT(2,1).

space by using a quaternion-based angular model of rigid origami for $a + b \leq 4$. Through numerical computation using a truss model, we computed solutions for larger integer pairs and found the volume-increasing nature of the folding. Finally, we showed the geometric connections between the geodesic folding of tetrahedra and other art forms, namely, triaxial weaving and zipper.

The construction in 3D leaves some open questions. First, the existence of intersection-free popped-up folded state for $a+b > 4$ remains as an open question. A different theoretical approach would be necessary for proving the existence in general. Assuming the existence, we also conjecture that the popped-up state is unique.

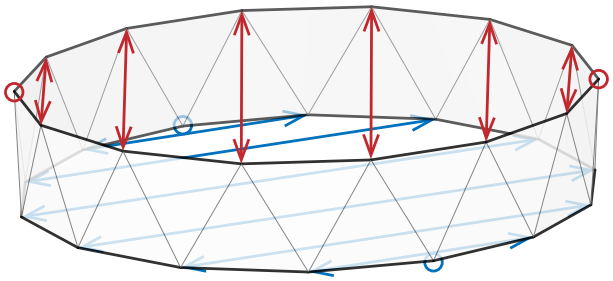

Figure 19: The loop that produces GFT(2,1). The vertices indicated by the arrows are attached by the zipper. The circles indicate the vertices of the base tetrahedron.

From the application viewpoint, the property that multiple shapes can be obtained from a common single strips of triangles may lead to a novel approach for fabricating programmable matters based on self-folding. We would like to further explore the variations of surfaces fabricated from the concept of geodesic strips.

Acknowledgment

This work started at an art-and-science-collaboration class "Individual and Group," directed by Tomohiro Tachi and Asao Tokolo, held at the University of Tokyo in February, 2019. We thank Asao Tokolo and other participants for their helpful comments. This work is supported by Japan Society for the Promotion of Science KAKENHIs 16H06106 and 20K21380 and Japan Science and Technology Agency PRESTO JPMJPR1927.

References

[1] Z. Abel, J. Cantarella, E. D. Demaine, D. Eppstein, T. C. Hull, J. S. Ku, R. J. Lang, and T. Tachi: *Rigid origami vertices: Conditions and forcing sets.* J. Comput. Geom. **7**(1), 2016. doi: 10.20382/jocg.v7i1a9.

[2] J. Akiyama: *Tile-makers and semi-tile-makers.* Amer. Math. Monthly **114**(7), 602–609, 2007. doi: 10.1080/00029890.2007.11920450.

[3] J. Akiyama and C. Nara: *Developments of polyhedra using oblique coordinates.* J. Indones. Math. Soc. **13**(1), 99–114, 2007. doi: 10.22342/jims.13.1.90.115-122.

[4] P. Ayres, A. G. Martin, and M. Zwierzycki: *Beyond the Basket Case: a principled approach to the modelling of Kagome weave patterns for the fabrication of interlaced lattice structures using straight strips.* In *Advances in Architectural Geometry 2018*, 72–93. Chalmers University of Technology, 2018.

[5] P. Ayres, A. Orlinski, M. Heimrath, S. Bornaz, and A. Martin: *Architectural Scale Kagome Weaving: Design Methods and Fabrication Concepts.* In *Fabricate 2020*, 178–185. 2020.

[6] S. Belcastro and T. Hull: *Modelling the folding of paper into three dimensions.* In *3rd International Meeting of Origami, Science, Math, and Education.* 2001.

[7] D. D. Bleecker: *Volume increasing isometric deformations of convex polyhedra.* J. Differential Geom. **43**(3), 505–526, 1996. doi: 10.4310/jdg/1214458323.

[8] D. L. Caspar and A. Klug: *Physical principles in the construction of regular viruses.* In *Cold Spring Harbor symposia on quantitative biology*, vol. 27, 1–24. Cold Spring Harbor Laboratory Press, 1962.

[9] E. D. Demaine, M. L. Demaine, A. Lubiw, and J. O'Rourke: *Enumerating foldings and unfoldings between polygons and polytopes.* Graphs Combin. **18**(1), 93–104, 2002. doi: 10.1007/s003730200005.

[10] E. D. Demaine and J. O'Rourke: *Geometric folding algorithms: linkages, origami, polyhedra.* Cambridge university press, 2007.

[11] P. Gailiunas: *Twisted Domes*. In *Bridges 2004: Mathematical Connections in Art, Music, and Science*, 45–52. Bridges Conference, 2004.

[12] P. Gailiunas: *A Mad Weave Tetrahedron*. In *Bridges 2011: Mathematics, Music, Art, Architecture, Culture*, 39–44. 2011.

[13] M. Kawamura: *Two Calculations for Geodesic Modular Works*. In *Origami^6: Sixth International Meeting of Origami Science, Mathematics, and Education, I: Mathematics*, 357–368. 2015.

[14] T. Kawasaki: $R(\gamma) = \mathbf{I}$. In *Proceedings of the Second International Meeting of Origami Science and Scientific Origami*, 31–40. 1997.

[15] C. Schüller, R. Poranne, and O. Sorkine-Hornung: *Shape representation by zippables*. ACM Trans. Graph. **37**(4), 1–13, 2018. doi: 10.1145/3197517.3201347.

[16] T. Tachi: *Simulation of rigid origami*. In *Origami^4: Fourth International Meeting of Origami Science, Mathematics, and Education*, 175–187. 2009.

[17] N. Tsuruta, J. Mitani, Y. Kanamori, and Y. Fukui: *Random Realization of Polyhedral Graphs as Deltahedra*. J. Geom. Graph. **19**(2), 227–236, 2015.

[18] W. Wu and Z. You: *Modelling rigid origami with quaternions and dual quaternions*. Proc. Roy. Soc. A: Math., Phys. Eng. Sci. **466**(2119), 2155–2174, 2010. doi: 10.1098/rspa.2009.0625.

Internet Sources

[19] F. M. Jackson: *Sequence A220171 in The On-Line Encyclopedia of Integer Sequences*, 2012. https://oeis.org/A220171.

[20] D. Piker: *K2Goals*. https://github.com/Dan-Piker/K2Goals.

[21] Wikipedia contributors: *Geodesic polyhedron — Wikipedia, The Free Encyclopedia*. https://en.wikipedia.org/wiki/Geodesic_polyhedron. [Online; accessed 14-October-2020].

[22] R. Zumkeller: *Sequence A198775 in The On-Line Encyclopedia of Integer Sequences*, 2011. https://oeis.org/A198775.

Received June 13, 2022; final form July 21, 2022.